

## Coulomb effects in the high-energy part of above-threshold-ionization spectra in intense bicircular laser fields

A. V. Sviridov<sup>1,2</sup>, M. V. Frolov<sup>1,2</sup>, S. V. Popruzhenko<sup>1,3</sup>, Lei Geng<sup>4</sup>, and Liang-You Peng<sup>4,5</sup>


<sup>1</sup>*Department of Physics, Voronezh State University, Voronezh 394018, Russia*

<sup>2</sup>*Department of Radiophysics, University of Nizhny Novgorod, Nizhny Novgorod 603950, Russia*

<sup>3</sup>*Prokhorov General Physics Institute of the RAS, Moscow 119991, Russia*

<sup>4</sup>*State Key Laboratory for Mesoscopic Physics and Frontiers Science Center for Nano-optoelectronics, School of Physics, Peking University, 100871 Beijing, China*

<sup>5</sup>*Peking University Yangtze Delta Institute of Optoelectronics, Nantong, Jiangsu 226010, China*

 (Received 26 April 2022; revised 11 August 2022; accepted 8 September 2022; published 28 September 2022)

Coulomb effects in the high-energy part of photoelectron spectra produced through the above-threshold ionization of an atom subject to intense short laser pulses are analyzed. The analysis is carried out for linearly polarized and tailored bicircular laser pulses consisting of the fundamental and the second-harmonic components. We include the Coulomb effects in the analytic semiclassical description of the photoelectron rescattering plateau using the recently developed adiabatic approach [*Phys. Rev. A* **104**, 033109 (2021)] and the expression for the Coulomb phase derived for description of the high harmonic generation [*J. Phys. B: At., Mol. Opt. Phys.* **51**, 144006 (2018)]. Comparisons between predictions of the analytic approach and numerical solutions of the time-dependent Schrödinger equation are presented. They allow the identification of the contribution of the Coulomb interaction to photoelectron spectra for different laser pulse forms. We show that the Coulomb effects appear more pronounced for bicircular fields, where they demonstrate considerable sensitivity to the photoelectron emission angle. Instead, for linear polarization, the Coulomb effect in the high-energy plateau is generally insignificant.

DOI: [10.1103/PhysRevA.106.033117](https://doi.org/10.1103/PhysRevA.106.033117)

### I. INTRODUCTION

Above-threshold ionization (ATI) of atoms in intense laser fields has remained in the focus of high-field physics for more than forty years, starting from experiment [1], where ATI photoelectron spectra were for the first time recorded. Continuous progress in laser techniques and diagnostics has been progressively offering new opportunities for detailed experimental investigation of photoelectron momentum distributions (PMDs). Advances in photoelectron and ion diagnostics made in the two past decades include the development of the velocity map imaging (VMI) [2] and the reaction microscope technique [3]. In combination with the progress in the generation and characterization of ultrashort laser pulses [4,5] this allowed for detailed investigations of a broad variety of ATI-associated effects with an unprecedented resolution. This includes the high-energy ATI (HATI) [6], high harmonic generation (HHG) [5,7,8], the low-energy structures in ATI spectra [9,10], effects of atomic structure in ATI and HHG [11–13], nondipole and magnetic-field effects [14], and more.

Over the past decade, ATI and HHG in tailored laser pulses have attracted the exceptional interest of researchers. This includes in particular ionization dynamics in laser fields of complex polarization states such as radially polarized pulses, twisted laser beams, beams with orbital momentum [15,16] and bicircular fields [8,17–19]. The latter is a coherent superposition of two circularly polarized fields of different

wavelengths. Most typically, in studies of ATI and HHG, bicircular fields consisting of  $\omega$  and  $2\omega$  components are used, where  $\omega$  is the laser frequency. An important feature of bicircular laser pulses is that their fields drive photoelectron trajectories of very different shapes. These shapes depend on the ionization time on the phase and amplitude relation between the two field components. As a consequence, in contrast to the case of monochromatic fields with circular or elliptical polarization, in bicircular fields returns of the photoelectron to its atomic residual become possible at different incident angles. Therefore, bicircular fields offer significant additional degrees of freedom for manipulation by HATI and HHG spectra. Recent results of experimental and theoretical studies of the recollision dynamics in intense bicircular fields have been reported in Refs. [20–26]; see also the literature quoted there.

The theory of ATI, HATI and HHG in intense laser fields employs three basic approaches: The Keldysh theory or strong-field approximation (SFA) [27–31], the adiabatic method [32–35], and the numerical solution to the time-dependent Schrödinger equation (TDSE). The SFA in its standard form discards the Coulomb interaction between the photoelectron and its parent ion, which limits its quantitative applicability to descriptions of negative ion multiphoton photodetachment. The same holds for the time-dependent effective range approach [36], which provides an analytic solution for an electron bound by a short-range forces in the presence of an intense laser field. In the limit of the zero-range

potential, the effective range approach provides an exact analytic solution for an electron in the field of a strong arbitrary polarized laser wave. Because of the discard of the Coulomb interaction, predictions of these model approaches may fail in describing experimental data and TDSE solutions for ATI and HHG in atoms. Such disagreements are commonly attributed to the effect of the Coulomb interaction. A broad variety of Coulomb effects in ATI and HHG have been studied theoretically, some of them have been experimentally verified. For reviews of Coulomb effects in strong-field ionization and methods applied to include the Coulomb interaction into approximate theoretical approaches, see Refs. [31,37] and references therein. These methods include, in particular, the Coulomb-corrected versions of the SFA [31,38,39] and the adiabatic approach based on the factorization of the ionization amplitude [35], which will be used for our current analysis.

The Coulomb interaction most significantly affects the dynamics of low-energy electrons produced through the direct ionization [27–31]. The energies of these slow electrons typically do not exceed the doubled ponderomotive energy and the corresponding low-energy part of the ATI spectrum, formed by multiple soft recollisions, is strongly modified by the Coulomb interaction [40–42]. HATI and HHG spectra are typically less affected by Coulomb effects and therefore in many cases they can be described within Coulomb-free analytic approaches. Qualitatively, this can be explained by the fact that the HATI and HHG plateaus are formed by fast electrons whose trajectories remain only slightly deformed by the Coulomb force. For HHG, the Coulomb effect was theoretically studied in Ref. [43]. It was shown there that the Coulomb modification of the high-harmonic phase is relatively small, although feasible. However, in the case of HHG, additional contributions of propagation effects may essentially screen or modify the Coulomb distortion of HHG spectra. In ATI, Coulomb effects are easier to trace, because of the single-atom nature of the ionization process. Detailed comparisons of HATI spectra calculated within Coulomb-free approaches with those extracted from TDSE numerical solutions demonstrate visible discrepancies. These deviations become more apparent in bichromatic fields, owing to a more complex form of photoelectron trajectories, such that different ionization times and trajectory shapes correspond to different emission angles. This makes ATI and HATI in bicircular fields capable of a much more detailed encoding of the ionization dynamics in photoelectron angular distributions. In combination with the existence of two-dimensional closed trajectories supporting recollisions, this offers an additional way of control of photoelectron dynamics in the presence of laser and the Coulomb fields.

In this paper, we explore this feature of the bichromatic fields and look for Coulomb effects in HATI spectra taking the case of linear polarization where these effects are less pronounced as a benchmark. At the same time, we do not focus on the Coulomb effects in the direct part of ATI spectra and spectra in circularly polarized fields, which have already received a detailed consideration (see recent publications [44–46], review [31]. and the literature therein). The paper is organized as follows: In the next section (Sec. II) we describe the theoretical methods used for the calculation of ATI and HATI spectra. These include (a) the adiabatic approach, (b) its

modification through the Coulomb corrections of the ionization amplitude, and (c) numerical TDSE solutions. Section III presents photoelectron spectra for different emission angles in the reference case of linear polarization and in a bichromatic field. In the same section, Coulomb effects are identified by comparisons between analytic and numerical calculations. Section IV contains summary and outlook. Appendixes A and B report technical details of the derivation of the direct and rescattering ionization amplitudes in the adiabatic limit.

## II. THEORETICAL METHODS FOR ABOVE THRESHOLD IONIZATION

In this section we give a short overview of the theoretical methods applied to our analysis of ATI. Details of these methods can be found in Refs. [34,35] for the adiabatic approach, and in Refs. [31,43,47] for the Coulomb corrections. Technical details of the TDSE numerical solution, which we will apply to benchmark our analytic results, can be found in Ref. [48].

### A. Adiabatic approach

The original formulation of the adiabatic approach is based on two assumptions: (i) the electron-atom interaction is approximated by a short-range potential, and (ii) the carrier frequency  $\omega$  and field strength  $F$  of a laser pulse are small compared with the corresponding atomic values ( $\omega \ll I_p$ ,  $F \ll (2I_p)^{3/2}$ ), where  $I_p$  is the atomic affinity (ionization potential). Here and below we use atomic units  $m = e = \hbar = 1$ . Within the adiabatic approach, the amplitude  $\mathcal{A}(\mathbf{p})$  of above-threshold detachment ATD is given by the sum

$$\mathcal{A}(\mathbf{p}) = \mathcal{A}^{(k)}(\mathbf{p}) + \mathcal{A}^{(r)}(\mathbf{p}), \quad (1)$$

where amplitudes  $\mathcal{A}^{(k)}(\mathbf{p})$  and  $\mathcal{A}^{(r)}(\mathbf{p})$  describe the subsequent levels of account of the atomic potential, and  $\mathbf{p}$  is the photoelectron final momentum. The lowest-order contribution is given by the amplitude  $\mathcal{A}^{(k)}(\mathbf{p})$ , also known in the literature as the Keldysh amplitude [27,30,31], while the term  $\mathcal{A}^{(r)}$  accounts for effects of a single additional interaction of the liberated electron with the atomic potential in the continuum. Each amplitude can be presented as a sum of partial contributions:

$$\mathcal{A}^{(\alpha)}(\mathbf{p}) = \sum_j \mathcal{A}_j^{(\alpha)}(\mathbf{p}), \quad \alpha = k, r, \quad (2)$$

where each  $\mathcal{A}_j^{(\alpha)}(\mathbf{p})$  is associated with a classical trajectory of a free electron in a laser pulse and expressed in terms of quantities parametrizing this trajectory. The partial amplitude  $\mathcal{A}_j^{(k)}(\mathbf{p})$ , mostly describing the low-energy photoelectron distribution, is parametrized by an outgoing trajectory with a given momentum of photoelectron far from the atom [31,44] (see also Appendix A). The partial amplitude  $\mathcal{A}_j^{(r)}(\mathbf{p})$ , describing “fast” (or rescattering) electrons, is expressed in terms of ionization and rescattering times, which parametrize a closed classical trajectory of a free electron in a laser field [34,35]. Under closed trajectories here we mean those arriving to parent ion space position at some time instant (referred to as “rescattering time” above) after the ionization event. This should not be confused with trajectories closed in energy or

momentum space. In the frame of the adiabatic approximation, the ionization ( $t'_j$ ) and recombination ( $t_j$ ) times are *real* solutions of a system of two transcendental equations:

$$\mathbf{K}'_j \cdot \dot{\mathbf{K}}'_j = 0, \quad (3a)$$

$$\frac{\mathbf{P}^2(t_j)}{2} - \frac{\mathbf{K}_j^2}{2} - \Delta\mathcal{E}_j = 0. \quad (3b)$$

Definitions for  $\mathbf{K}'_j$ ,  $\dot{\mathbf{K}}'_j$ ,  $\mathbf{P}(t_j)$ ,  $\mathbf{K}_j$ ,  $\Delta\mathcal{E}_j$  can be found in Appendix B. These equations represent semiclassical conditions, which make possible realization of the rescattering mechanism for the ATD process [49]: Equation (3a) shows that the atomic electron appears in the laser-dressed continuum at the moment, which ensures the minimum of the kinetic energy; Eq. (3b) indicates that the rescattering event happens for those moments, when the energy gained by the electron during its motion along a closed trajectory equals the energy of the ionized electron with a given final momentum.

The amplitude  $\mathcal{A}_j^{(k)}(\mathbf{p})$  is parametrized in terms of a classical action of a free particle and the tunneling exponent (see Appendix A), which identifies the mechanism of the nonlinear detachment. More complex parametrization is obtained within the adiabatic approach for the amplitude  $\mathcal{A}_j^{(r)}(\mathbf{p})$ . This amplitude is presented as the product of three factors (see Appendix B) describing tunneling, propagation, and elastic rescattering on the atomic potential, which is the third step in the recollision scenario.

Once the amplitude  $\mathcal{A}(\mathbf{p})$  is found analytically, the momentum distribution of photoelectrons can be calculated as

$$\mathcal{P}(\mathbf{p}) \equiv \frac{d^3W(\mathbf{p})}{dE_p d\Omega_p} = \frac{p}{(2\pi)^3} |\mathcal{A}(\mathbf{p})|^2, \quad (4)$$

where  $E_p = p^2/2$  and  $\Omega_p$  is the solid angle of the photoelectron emission. Note that the geometry of the momentum vector  $\mathbf{p}$  in Eq. (4) is uniquely determined by the energy  $E_p$  and solid angle  $\Omega_p$ , so that for shortness of notation in the subsequent analysis we use the abbreviation  $\mathbf{p} \equiv (E_p, \Omega_p)$ : e.g., for the linearly polarized field  $\Omega_p = (\theta_p \equiv \theta, \varphi_p = 0)$ ,  $\theta_p$  and  $\varphi_p$  are spherical angles; for the bicircular field  $\Omega_p = (\theta_p = \pi/2, \varphi_p \equiv \theta)$ . Below, we refer to the outcome of this adiabatic approach as the adiabatic result (AR), while results obtained with the reduced amplitude,  $\mathcal{A}(\mathbf{p}) \approx \mathcal{A}^{(k)}(\mathbf{p})$  are denoted as the Keldysh result (KR).

## B. Coulomb corrections

Results obtained within the aforementioned adiabatic approach cannot be directly utilized to describe ionization of atoms because it does not account properly for the long-range Coulomb interaction. Even the electron-scattering amplitude cannot be calculated within the standard expression for a short-range potential [see Eq. (B5)] and requires a special consideration [50]. Moreover, the Coulomb field affects the ionization process of an atomic system by considerably enhancing the total ionization yield [51,52] and changing the photoelectron momentum distributions [40,53,54]. Therefore, the amplitudes  $\mathcal{A}_j^{(k)}$  and  $\mathcal{A}_j^{(r)}$  need a Coulomb modification. The amplitude  $\mathcal{A}_j^{(k)}$  is modified by introducing the exponential Coulomb-induced correction [31,38,40,47], while correcting

the amplitude  $\mathcal{A}_j^{(r)}$  is more laborious: It requires (i) changing the electron-scattering amplitude to the corresponding atomic counterpart calculated numerically or analytically for a hydrogen-like atom [50], and (ii) introducing a special exponential Coulomb-induced correction along a closed photoelectron trajectory [43].

The Coulomb-induced factor in the amplitude  $\mathcal{A}_j^{(k)}$  is given by the expression

$$Q_j^{(k)} = e^{i\Phi_j^{(k)}}, \quad (5)$$

where the phase  $\Phi_j^{(k)}$  is expressed through a one-dimensional integral in the complex time plane [43,47]:

$$\Phi_j^{(k)} = \int_{t_j^{(k)}}^{\tau} dt \left[ \frac{1}{\sqrt{\mathbf{r}_j^{(k)}(t) \cdot \mathbf{r}_j^{(k)}(t)}} + \frac{i\nu}{t - t_j^{(k)}} \right], \quad (6a)$$

$$\mathbf{r}_j^{(k)}(t) = \mathbf{p}(t - t_j^{(k)}) + \int_{t_j^{(k)}}^t \mathbf{A}(t') dt', \quad (6b)$$

$$\frac{1}{2} [\mathbf{p} + \mathbf{A}(t_j^{(k)})]^2 + I_p = 0, \quad \nu = \frac{Z}{\kappa}, \quad (6c)$$

and  $t_j^{(k)} \approx \bar{t}_j + i\bar{\varkappa}_j/\bar{\mathcal{F}}_j$  is the complex transition moment from the bound state to the continuum state (see the definitions of  $\bar{t}_j$ ,  $\bar{\varkappa}_j$ , and  $\bar{\mathcal{F}}_j$  in Appendix A),  $\tau$  is the moment that the laser pulse is turned off,  $Z$  is the atomic residual charge ( $Z = 1$  for ionization of a neutral atom). Note that the integration path is chosen to avoid crossings with the integrand branch cuts to make it a single-valued function.<sup>1</sup> Below we refer results obtained with the Coulomb-corrected Keldysh amplitude as the Coulomb-corrected Keldysh result (CCKR).

The corresponding Coulomb-induced factor for the amplitude  $\mathcal{A}_j^{(r)}$  is derived within the procedure suggested in Ref. [43] (see also Ref. [55]) and presented by the expression:

$$Q_j^{(r)} = e^{i\Phi_j^{(r)}}, \quad \Phi_j^{(r)} = \int_{t_j^{(r)}}^{t_j} \left[ \frac{1}{\sqrt{\mathbf{r}_j^{(r)}(t) \cdot \mathbf{r}_j^{(r)}(t)}} + \frac{i\nu}{t - t_j^{(r)}} - \frac{\nu}{t - t_j} \right] dt, \quad (7a)$$

$$\mathbf{r}_j^{(r)}(t) = \int_{t_j^{(r)}}^t \mathbf{A}(t') dt' - \frac{t - t_j^{(r)}}{t_j - t_j^{(r)}} \int_{t_j^{(r)}}^{t_j} \mathbf{A}(t') dt', \quad (7b)$$

$$t_j^{(r)} = t'_j + i\kappa_j/\mathcal{F}_j, \quad (7c)$$

where equations for times  $t'_j$  and  $t_j$  expressions for  $\kappa_j$  and  $\mathcal{F}_j$  are given in Appendix B. Similarly to (6a), the integral in Eq. (7a) is taken in the complex-time plane avoiding crossing with the branch cuts.

Extension of analytic results obtained within the adiabatic approximation to neutral atoms or positively charged ions is achieved by multiplication of the amplitudes  $\mathcal{A}_j^{(k)}$  and  $\mathcal{A}_j^{(r)}$  to the corresponding Coulomb-induced factors and

<sup>1</sup>The branch cut crossing changes the sign of the potential, thereby changing an attractive potential to a repulsive one.

replacing the electron-scattering amplitude by the corresponding atomic counterpart. Below we call the sum of the two Coulomb-corrected amplitudes  $\mathcal{A}^{(k)}(\mathbf{p})$  and  $\mathcal{A}^{(r)}(\mathbf{p})$  the Coulomb-corrected adiabatic result (CCAR).

### C. Numerical solution of time-dependent Schrödinger equation

For the numerical solution of TDSE, we use the velocity gauge and dipole approximation for the electron-laser interaction:

$$i \frac{\partial}{\partial t} \Psi(\mathbf{r}, t) = \hat{H} \Psi(\mathbf{r}, t), \quad \hat{H} = -\frac{\nabla^2}{2} - \frac{1}{r} - i\mathbf{A}(t) \cdot \nabla, \quad (8)$$

where  $\mathbf{A}(t)$  is the vector potential of the laser field. The time-dependent wave function is expanded in terms of spherical harmonics  $Y_{lm}(\hat{\mathbf{r}})$  for angular coordinates:

$$\Psi(\mathbf{r}, t) = \frac{1}{r} \sum_{l=0}^{l_{\max}} \sum_{m=-l}^{m=l} \psi_{lm}(r, t) Y_{lm}(\hat{\mathbf{r}}), \quad (9)$$

with  $\hat{\mathbf{r}} = \mathbf{r}/r$ . We choose  $l_{\max} = 130$  to ensure convergence of the result. The finite element discrete variable representation (FE-DVR) is used to discretize the radial coordinate  $r$  [56]. The entire coordinate space, ranging from zero to  $r_{\max} = 240$  a.u., is partitioned into 112 finite elements. We have checked the convergence of our calculation by doubling the grid size and found no visible differences. Legendre-Gauss-Lobatto quadratures of order eight are employed in every finite element. The ground state of the hydrogen atom is prepared numerically by the restarted Lanczos algorithm. Otherwise, we use the Arnoldi propagator to carry out the evolution of the wave function [57]. To save computational time and reduce the reflection effect, the splitting scheme is used for the wave function  $\Psi(\mathbf{r}, t)$  [58]:

$$\Psi = \Psi_{\text{inner}} + \Psi_{\text{outer}} = M\Psi + (1 - M)\Psi. \quad (10)$$

The wave function is split by a mask function  $M$ :

$$M(r) = \frac{1}{1 + \exp\left(\frac{r-r_c}{r_w}\right)}, \quad (11)$$

where  $r_c = 0.5r_{\max}$  and  $r_w = 0.03r_{\max}$ . Every one-third of the laser cycle at time  $t_i$ ,  $\Psi_{\text{outer}}$  is separated, which is then projected to the scattering states and analytically propagated until the end of the pulse  $t_f$  by using the Volkov propagator,

$$U_V(t_f, t_i) = \exp\left[-iE(t_f - t_i) - i \int_{t_i}^{t_f} \mathbf{p} \cdot \mathbf{A}(\tau) d\tau\right]. \quad (12)$$

The residual wave function  $\Psi(\mathbf{r}, t_f)$  is also projected to the scattering states after the laser pulse is turned off. Finally, the split wave function and the residual wave function are coherently added up in the momentum space to calculate the double-differential probability:

$$\begin{aligned} \mathcal{P}(\mathbf{p}) &= \frac{d^3 W(\mathbf{p})}{dE_p d\Omega_p} \\ &= \frac{1}{2\pi p} \left| \sum_{l,m} (-i)^l e^{i\delta_l} Y_{lm}(\hat{\mathbf{p}}) \int_0^\infty dr \psi_{lm}^{\text{all}}(r, t_f) r R_{pl}(r) \right|^2, \end{aligned} \quad (13)$$

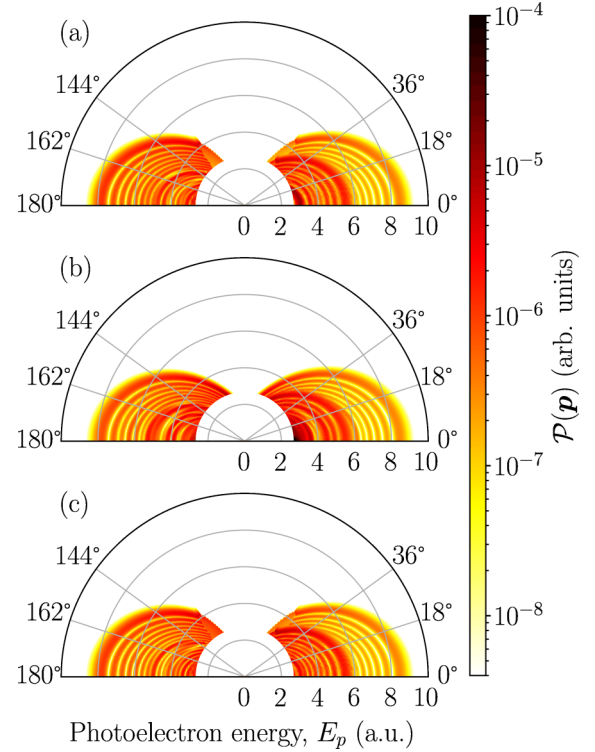


FIG. 1. Color-coded angle-resolved ATI spectra for the linearly polarized field (15). The polarization direction ( $z$  direction) is horizontal. Because of the symmetry of the distribution with respect to this direction, only upper half planes ( $p_y > 0$ ) are shown. The low-energy part of the distributions is not shown (empty circle at photoelectron energies  $E_p < 2.5$  a.u.). Panel (a) shows the AR result. Panel (b) shows the TDSE-result. Panel (c) shows the CCAR result. For laser parameters see the text.

$$\psi_{lm}^{\text{all}}(r, t_f) = \sum_{t_i} U_V(t_f, t_i) \psi_{lm}^{\text{outer}}(r, t_i) + \psi_{lm}(r, t_f), \quad (14)$$

where  $\hat{\mathbf{p}} = \mathbf{p}/p$  defines the photoelectron momentum direction,  $\delta_l$  stands for the Coulomb phase shift, and  $R_{pl}$  stands for the Coulomb scattering states in the radial coordinate  $r$ , both functions are described by analytic expressions.

### III. RESULTS AND DISCUSSION

In Figs. 1 and 2 we present two-dimensional (2D) ATI momentum distributions found for linearly polarized and bicircular laser pulses using the above-described approaches. For linear polarization the field was taken in the form

$$\mathbf{A}(t) = \begin{cases} -\hat{z} \frac{F}{\omega} \cos^2\left(\frac{\pi t}{\tau}\right) \cos(\omega t), & |t| \leq \tau/2 \\ 0, & \text{otherwise,} \end{cases} \quad (15)$$

while the bicircular pulse was parametrized as

$$\mathbf{A}(t) = \frac{\partial \mathbf{R}(t)}{\partial t}, \quad \mathbf{R}(t) = \mathbf{R}_1(t) + \mathbf{R}_2(t), \quad (16a)$$

$$\mathbf{R}_i = \frac{F}{\omega_i^2} f_i(t) (\hat{x} \cos \omega_i t + \eta_i \hat{y} \sin \omega_i t), \quad (16b)$$

$$f_i(t) = \exp(-2(\ln 2)t^2/\tau_i^2). \quad (16c)$$



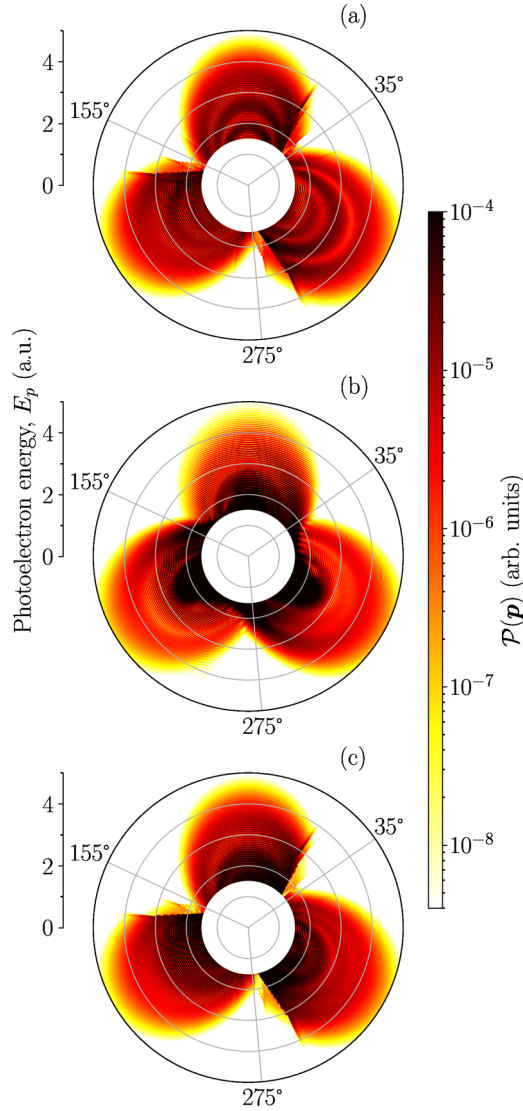


FIG. 2. Color-coded angle-resolved ATI spectra for the bicircular field (16) in the polarization plane. The  $x$  axis is horizontal, the  $y$  axis is vertical. The low-energy part of the distributions is not shown (empty circle at photoelectron energies  $E_p < 1.5$  a.u.). Panel (a) shows the AR result. Panel (b) shows the TDSE-result. Panel (c) shows the CCAR result. See text for laser parameters.

For Eq. (15),  $F = 0.0654$  a.u. is the laser field strength corresponding to the intensity  $I = cF^2/(8\pi) = 1.5 \times 10^{14}$  W/cm<sup>2</sup>,  $\omega = 0.035$  a.u. is the pulse carrier frequency corresponding to the wavelength  $\lambda = 2\pi c/\omega = 1.3$   $\mu$ m,  $c$  is the speed of the light,  $\tau = 26$  fs is the full duration of the six-cycle pulse. For Eq. (16),  $F = 0.0534$  a.u. corresponding to the intensity  $I = 1 \times 10^{14}$  W/cm<sup>2</sup>,  $\omega_i$  are the carrier frequencies of the bicircular field components  $\omega_1 = \omega_2/2 = 0.057$  a.u.,  $\eta_i$  are the ellipticities ( $\eta_1 = -\eta_2 = 1$ ) and the full width at half maximum of the intensity pulse durations are  $\tau_i = 2\pi N_i/\omega_i$  with  $N_1 = 2$ ,  $N_2 = 4$ . All calculations were performed for hydrogen in the initial  $1s$  state. Results shown in Figs. 1 and 2 were obtained by the TDSE numerical solution (TDSE result), in the adiabatic approximation with the Coulomb interaction

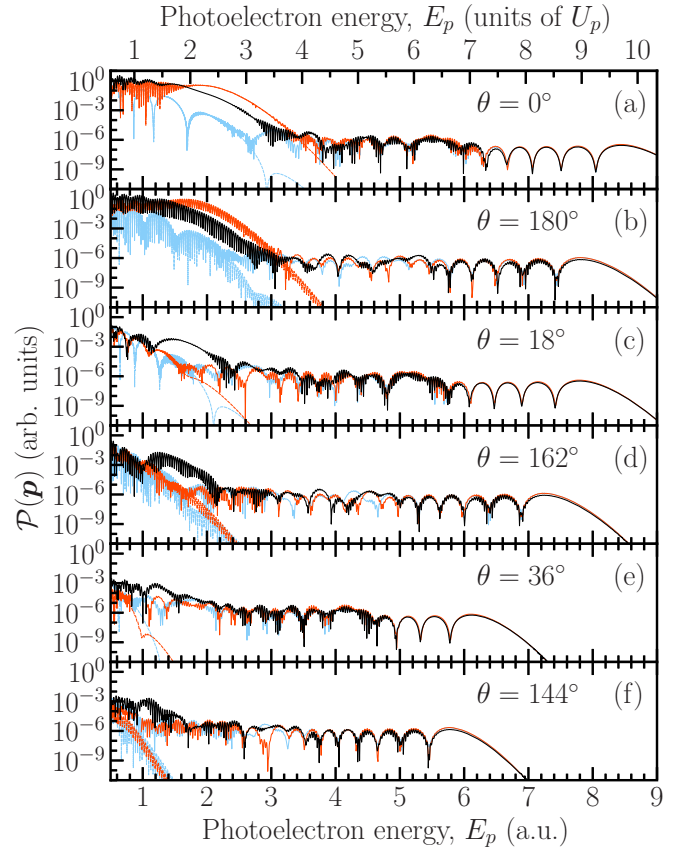


FIG. 3. ATI spectra for the hydrogen in the linearly polarized field [see the text for laser parameters and Eq. (15) for parametrization] calculated for six photoelectron emission angles  $\theta$  with respect to the polarization vector  $\hat{z}$  (indicated in Fig. 1 by thin radial lines). The values of  $\theta$  are marked in the panels. Photoelectron energies are shown both in atomic units and in units of the ponderomotive energy. Black solid lines show TDSE result; blue solid lines show AR; blue dashed lines show KR; red solid lines show CCAR; red dashed lines show CCKR.  $U_p = F^2/(4\omega^2) \approx 0.87$  a.u.

neglected (adiabatic result—AR) and within the Coulomb-corrected adiabatic approximation (CCAR).

Since we focus on the Coulomb effect for the high-energy part of the photoelectron distributions, in Figs. 1 and 2 we do not show the low-energy domain known in the literature as the direct ionization spectrum (for Fig. 1 this domain is limited by  $E_p < 2.5$  a.u., for Fig. 2,  $E_p < 1.5$  a.u.). (We show the contribution of the low-energy part in Figs. 3 and 4.) The central message of the distribution shown in Figs. 1 and 2 is that the Coulomb effect on the high-energy part of the spectrum is much less pronounced in the case of linear polarization than for a bicircular pulse. Indeed, for linear polarization, the AR and CCAR distributions [see Fig. 1(a) and 1(c), respectively] look almost identical and both of them match with results in Fig. 1(b). For the bicircular field, the TDSE result [see Fig. 2(b)] and the CCAR [see Fig. 2(c)] appear qualitatively more similar to each other than the AR distribution in Fig. 2(a). In particular, both distributions in Figs. 2(b) and 2(c) show areas of enhanced ionization probability in forms of three leafs at photoelectron energies 1.5–3.0 a.u. Also, the TDSE and CCAR distributions

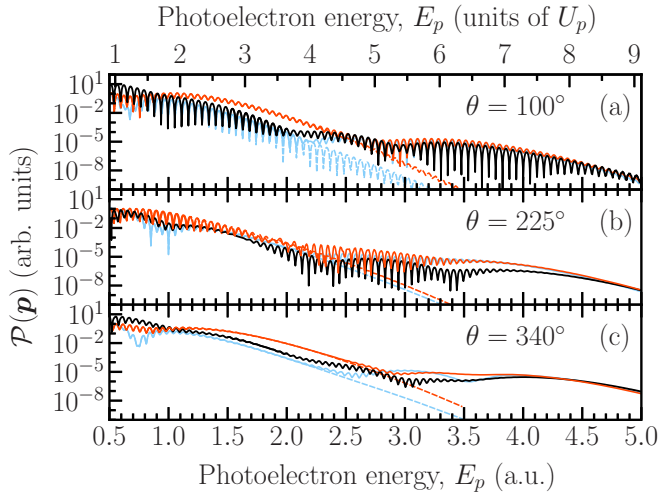


FIG. 4. ATI spectra for the hydrogen atom in the bicircular field [see the text for laser parameters and Eq. (16) for parametrization] calculated in the polarization plane ( $XY$  plane) for different photoelectron emission angles  $\theta$  with respect to  $\hat{x}$  vector. Photoelectron energies are shown both in atomic units and in units of the ponderomotive energy. Black solid lines show TDSE-result; blue solid lines show AR; blue dashed lines show KR; red solid lines show CCAR; red dashed lines show CCKR.  $U_p = F^2/(2\omega_1^2) + F^2/(2\omega_2^2) \approx 0.55$  a.u.

demonstrate a less pronounced interference pattern than shown in Fig. 2(a) for the AR distribution. These qualitative observations allow us to conclude that for bicircular laser fields the Coulomb interaction makes a stronger effect on the structure of the high-energy photoelectron plateau, compared with the case of linear polarization where this effect remains hardly visible.

To provide a more detailed quantitative consideration of this Coulomb effect we present in Figs. 3 and 4 ATI spectra for several fixed emission angles. Except for the above-mentioned TDSE, AR, and CCAR results we also show the Keldysh Coulomb-free result (KR) and its Coulomb-corrected version (CCKR).

Our numerical results for the linearly polarized pulse show that the Coulomb factor (5) for the partial amplitudes  $\mathcal{A}_j^{(k)}$  changes the low-energy part of the ATI spectra. However, its inclusion does not provide quantitative agreement between the analytic approach and the numerical TDSE solution. In the best case, the Coulomb factor yields some quantitative improvement. First, it leads to the development of the low-energy plateau with an overestimated magnitude near the low-energy cutoff [see Figs. 3(a) and 3(b)]. This effect received a detailed consideration in Ref. [54]. Secondary, the Coulomb factor corrects the phase of the partial ionization amplitude  $\mathcal{A}_j^{(k)}$ , thereby forming the large-scale interference structure in the ATI spectra at low energies [see Figs. 3(c) and 3(d)]. We observe significant discrepancies between predictions of the analytic approach and numerical TDSE results in the range 1–3 a.u., where the partial rescattering amplitudes  $\mathcal{A}_j^{(r)}$  do not yet contribute. As we do focus here on the low-energy part of the photoelectron distributions but consider effects of the Coulomb interaction in the high-energy plateau, we limit

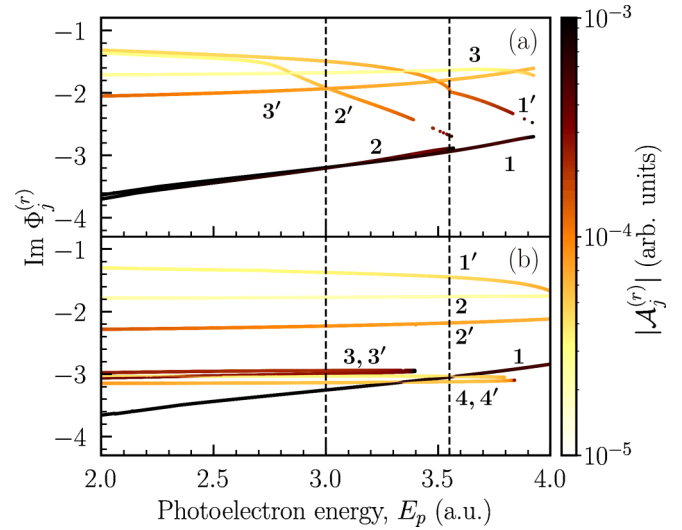


FIG. 5. Dependence of the imaginary part of  $\Phi_j^{(r)}$  on the photoelectron energy for two photoionization angles: (a)  $\theta = 100^\circ$ , (b)  $\theta = 340^\circ$ . Parameters of the bicircular field are the same as in Fig. 4. Each line corresponds to a particular closed trajectory, while its continuously changing color marks the absolute value of the partial amplitude  $\mathcal{A}_j^{(r)}$ . Vertical dashed lines indicate two photoelectron energies:  $E_p = 3$  a.u. and  $E_p = 3.55$  a.u.

our discussion of the low-energy electrons by the following brief comments: (i) The discrepancies may be attributed to an incomplete account of the Coulomb-distorted trajectories, which can be additionally induced by the Coulomb field [59–61]. Such new trajectories do not appear in our calculation based on the Coulomb-free ones. (ii) The disagreement may result from a more fundamental reason, which potentially roots to the inconsistency of the expression (1) establishing the explicit separation of the ionization amplitude in the rescattering and Keldysh-like contributions, which may not be applicable in the presence of the long-range Coulomb field. Note that a similar problem is known in scattering theory, where the laser-free continuum states are separable into the plane and the scattering parts for a short-range potential, while for Coulomb continuum states this cannot be done [50,62]. The high-energy part of ATI spectra for the linearly polarized pulse (see Fig. 3) is less sensitive to the Coulomb corrections (7). Indeed, excluding some energies, the TDSE results, analytic results with and without Coulomb factors are found in good agreement with each other. For those small energy intervals where we observe discrepancies between the TDSE and the Coulomb-free analytic results, the factor (7) improves the agreement. Note that, for backscattered electrons ( $\theta = 0^\circ, 180^\circ$ ), the plateau cutoff position is slightly shifted toward lower energies with respect to the commonly expected value of  $10U_p$ . This can be explained by the finite pulse duration  $\tau = 26$  fs. Indeed, the instant field amplitude and the ponderomotive energy upon the first photoelectron return to the nucleus appear below their peak values [63].

ATI spectra for the bicircular field (16) are presented in Fig. 4. In contrast to the case of the linearly polarized field, the low-energy parts of the ATI spectra are in good agreement with numerical TDSE results showing a gradual decrease

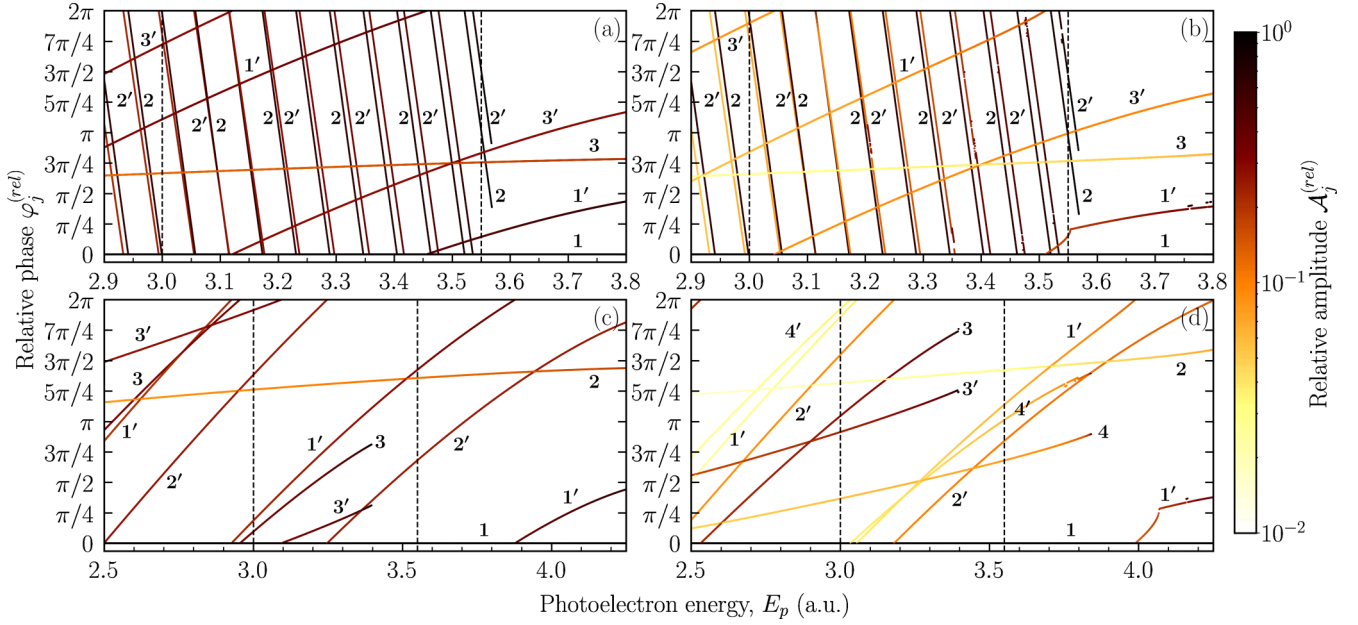


FIG. 6. Phase dependence of the partial amplitudes on the photoelectron energy. Continuously changing color along the curves indicates the relative absolute value of the partial amplitude. Labeling of the partial amplitudes (and of the corresponding classical trajectories) is the same as in Fig. 5. (a) Ionization angle  $\theta = 100^\circ$ , the Coulomb corrections are not included. (b) Ionization angle  $\theta = 100^\circ$ , the Coulomb corrections are included. (c) Ionization angle  $\theta = 340^\circ$ , the Coulomb corrections are not included. (d) Ionization angle  $\theta = 340^\circ$ , the Coulomb corrections are included. Parameters for the bicircular field are the same as in Fig. 4. Vertical dashed lines mark energies  $E_p = 3$  a.u. and  $E_p = 3.55$  a.u.

of the photoelectron yield with increasing energy. Note, however that in this study we focus on high-energy photoelectron spectra. The rescattering part of the ATI amplitude generates a shorter (compared with the case of linear polarization) plateau, which ends up by a smoothly decreasing tail. As can be seen from Fig. 4, the Coulomb corrections contribute differently for different emission angles. For instance, for two ionization angles  $\theta = 100^\circ$  and  $\theta = 225^\circ$  [Figs. 4(a) and 4(b)] the Coulomb factor (7) makes a minor contribution to the high-energy plateau structure, while for  $\theta = 340^\circ$  [Fig. 4(c)] it smears out a large-scale oscillation in the plateau region. Note that the Coulomb factor enhances the absolute value of the partial amplitudes. For consistency, the ionization yield in the absence of the Coulomb correction was properly scaled to the Coulomb-corrected results.

In Fig. 5 we present the dependence of the imaginary part of  $\Phi_j^{(r)}$  [see Eq. (7a)] on the photoelectron energy for the most contributing trajectories and two ionization angles [ $\theta = 100^\circ$ , Fig. 5(a), and  $\theta = 340^\circ$ , Fig. 5(b)]. The contributing trajectories are combined in pairs in such a way that each pair merges at the same energy. In a linearly polarized field, such pairs turn into the well-known short and long trajectories. Each pair is marked by a number, while within the pair the second trajectory is additionally marked by a prime. Within a pair, contributions of the trajectories can considerably differ in absolute value. As an example, in Fig. 5(a) the contribution of trajectory “2” is much higher than that of trajectory “2’”. The imaginary part of  $\Phi_j^{(r)}$  [see Eq. (7a)] determines the Coulomb-induced enhancement or suppression of the contribution of a partial amplitude  $\mathcal{A}_j^{(r)}$  [see Eq. (7)]. In combination with the

tunneling factor of  $\mathcal{A}_j^{(r)}$  [see Eq. (B3)] this determines the contribution of a particular trajectory to the ionization amplitude.<sup>2</sup> For  $\theta = 100^\circ$  [see Fig. 5(a)] there are two contributing trajectories (see lines marked by “1” and “2”), whose Coulomb factors enhance the corresponding partial amplitudes. Coherent summation of these amplitudes generates the interference pattern with  $\omega$ -separated peaks. Note that these peaks should not be associated with ATI peaks, since their position and appearance depend on the ionization angle. As an example, for  $\theta = 340^\circ$  [see Fig. 5(b)] there is only one contributing trajectory and the plateau structure for this angle does not demonstrate any interference pattern. The traveling time (i.e., the difference  $t_j - t'_j$ ) of the most contributing trajectories is near one third of the laser period,  $2\pi/\omega$ .

Figures 5 and 6 can help to shed further light on the formation of the large-scale interference structure and on the Coulomb effect on this structure. The dependence of the relative phases and magnitudes of the partial amplitudes  $\mathcal{A}_j$  on the photoelectron energies is presented in Fig. 6. The absolute value of the partial amplitude is shown by continuously changing color along the curve associated with a given partial amplitude  $\mathcal{A}_j$  plotted in the “energy-phase” plane. Figures 6(a) and 6(b) show the phase dependence for the case of pronounced interference structure in ATI spectra for  $\theta = 100^\circ$ . In both cases of AR [Fig. 6(a)] and CCAR

<sup>2</sup>See the amplitude suppression in Fig. 5(a) for trajectory “3,” whose phase imaginary part is less than the corresponding part of  $\Phi_j^{(k)}$  for trajectory “1’.”

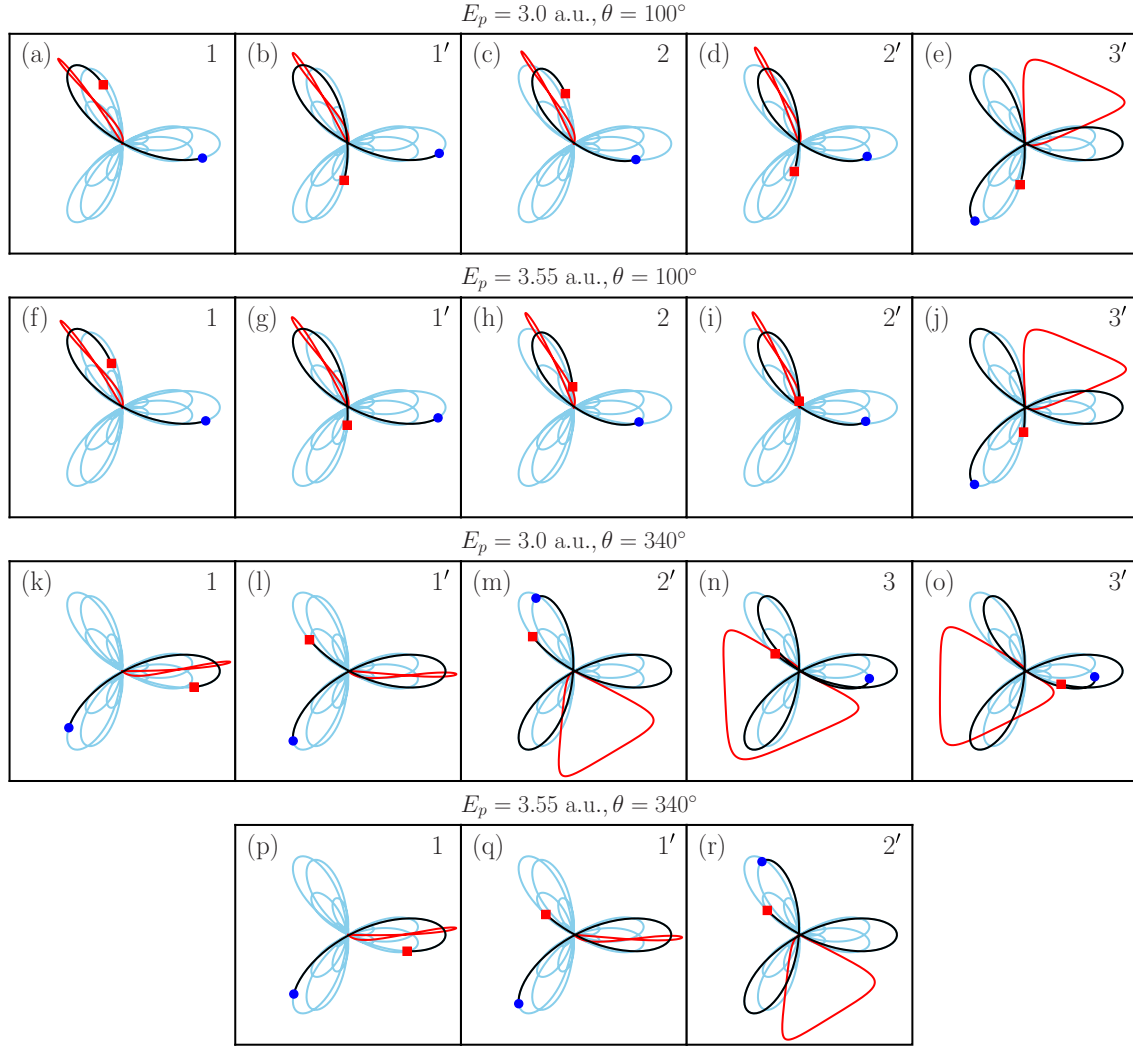


FIG. 7. 2D graphs of the dominant closed classical electron trajectories for different energies and ionization angles as marked in the figure. Red lines show closed classical electron trajectories (the electron moves counterclockwise). Black lines show the corresponding electric-field hodograph (black line) drawn from the instant of ionization (blue circle) to that of recombination (red square). Thin blue lines show the electric-field hodograph for the entire pulse.

[Fig. 6(b)] the interference structure results from coherent summation of the mostly contributing trajectories marked as “1” and “2.” The relative phases of trajectories “2” are reduced to the interval  $[0, 2\pi]$  so that the corresponding curves form sloping discontinued lines separated by  $\omega$ . Consequently, their coherent summation forms an  $\omega$ -spaced interference structure. Note that two trajectories “2” and “2'” contribute almost equally to the interference with the trajectory “1,” while for CCAR the dominant contribution comes from trajectory “2.” For  $\theta = 340^\circ$  the topological shape of the phase dependence changes dramatically. The phase of the partial amplitudes for trajectories “2” and “2'” changes its slope and the corresponding discontinued lines are separated by energy intervals exceeding  $\omega$ . At the same time, the contribution of the partial amplitudes associated with trajectories “2” and “2'” becomes less pronounced in comparison with the amplitude “1.” These two effects lead to suppression of interference effects in the

plateau region [see Fig. 4(c)]. As we can see from our numerical analysis, for this ionization angle the Coulomb effects appear much more pronounced than for  $\theta = 100^\circ$ . The shapes of several most contributing trajectories are shown in Fig. 7.

We attribute the observed selectivity of the Coulomb corrections to the ionization angle to the short time duration of the bicircular pulse. Indeed, for a monochromatic bicircular field interference of partial amplitudes of the same type leads to the appearance of  $E_p$ -dependent  $\delta$  functions, determining positions of the ATI peaks. For a short pulse, each partial amplitude and the corresponding classical trajectory have individual forms suppressing the development of the ideal ATI comb. As a consequence, the Coulomb factors come with different weights and change the interference pattern.

For better visualization of the contributions of different partial amplitudes  $\mathcal{A}_i^{(r)}$ , we plot them as vectors with length and angle given by the absolute value and the phase of the



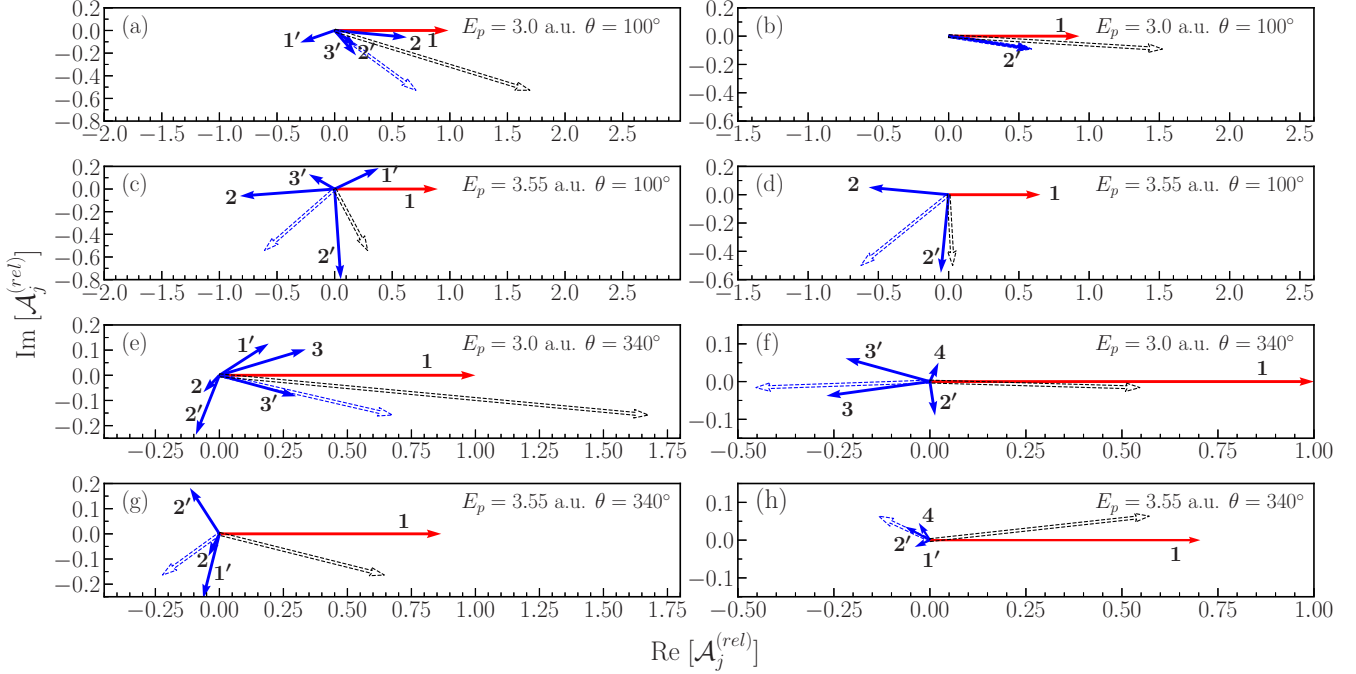


FIG. 8. Schematic representation of partial ionization amplitudes. Solid red vectors show the most contributing partial amplitudes, solid blue vectors show the remaining contributing amplitudes, dashed black vectors show the total ionization amplitudes, dashed blue vectors show the sum of the remaining contributing amplitudes. Panels (a), (c), (e), (g) show diagrams of the partial amplitudes without the Coulomb corrections, panels (b), (d), (f), (h) show diagrams of the partial amplitudes with the Coulomb corrections. Numbers mark trajectories associated with the corresponding partial amplitudes as in Fig. 5. Photoelectron energies and emission angles are presented in the figures. The bicircular field parameters are the same as in Fig. 4.

considered partial amplitude (Fig. 8). The offset angle is chosen zero for the most contributing trajectory. The left-hand side (right-hand side) of Fig. 8 shows the partial amplitudes without (with) the Coulomb factor (7). We consider two photoelectron energies (marked in Fig. 5 by dashed vertical lines) and two photoionization angles  $\theta = 100^\circ$  and  $\theta = 340^\circ$ . To exclude the difference in absolute ionization yields caused by the Coulomb factors we scale the Coulomb-free results [see Figs. 8(a), 8(c), 8(e), and 8(g)] by the factor  $3.8 \times 10^{-5}$ , thereby reducing the length of the red vector (corresponding to the most contributing partial amplitudes) in Fig. 8(g) to one. The corresponding scaling factor for Figs. 8(b), 8(d), 8(f), and 8(h) is  $9.8 \times 10^{-4}$ . In all cases the Coulomb corrections crucially change the relative contribution of different partial amplitudes by changing both their absolute values and relative phases. However, the modification of the partial amplitudes caused by the Coulomb effect does not necessarily affect the ionization yield. These special cases can also be found in Figs. 8(a)–8(d). They correspond to the situation when the sum of the remaining partial amplitudes (see blue vectors in Fig. 8) is not significantly changed by the Coulomb corrections. For those ionization angles where the Coulomb corrections are significant [see Figs. 8(e)–8(h)] we observe a considerable change in the resulting sum of the remaining partial amplitudes. This change is mostly caused by the Coulomb correction to the phase, while the change in the absolute value plays a secondary role. As a result, we observe the interference-related suppression or increase of the total ionization probability.

#### IV. SUMMARY

In this work, we have analyzed the Coulomb field effects for high-energy electrons produced through the nonlinear ionization of an atom subject to intense linearly polarized and bicircular laser fields. The Coulomb factors for rescattered electrons were introduced within the adiabatic approach [35] by extending the semiclassical method previously developed in Ref. [43] for description of high-harmonic spectra, to the HATI case. Two types of short laser pulses were considered: A linearly polarized pulse and a tailored bicircular pulse with  $\omega$  and  $2\omega$  components and counter-rotating circular polarizations. Although the introduced Coulomb corrections improve the agreement between analytic results and numerical solutions of TDSE in both cases, the improvement is considerably more apparent for the tailored bicircular pulse, while for the linearly polarized field the Coulomb correction reduces to the common factor weakly dependent on the photoelectron energy. We show that coherent summation of different partial amplitudes associated with spatially closed classical trajectories in the bicircular pulse can be considerably affected by the Coulomb corrections changing both the absolute values and the phases of these amplitudes. This significantly modifies the interference pattern in the high-energy photoelectron plateau. In a linearly polarized field the effects of multiple returns and of soft recollisions both discarded in our consideration are known to significantly influence the photoelectron spectra. Highly likely, this is the reason why in linearly polarized fields

our adiabatic Coulomb-corrected approach appears less efficient.

### ACKNOWLEDGMENTS

This work was supported in part by the Ministry of Education and Science of the Russian Federation through Project No. FZGU-2020-0035, trajectory analysis was performed within grant of Russian Science Foundation (Project No. 20-11-20289).

### APPENDIX A: THE “DIRECT” AMPLITUDE $\mathcal{A}_j^{(k)}$

The partial “direct” amplitude  $\mathcal{A}_j^{(k)}$  can be calculated along the expressions

$$\mathcal{A}_j^{(k)} = f(\mathbf{p}) e^{iS(\mathbf{p}, \bar{t}_j)} e^{-\frac{\bar{\varkappa}_j^3}{3\bar{\mathcal{F}}_j}}, \quad (\text{A1a})$$

$$\mathbf{P}(\bar{t}_j) \cdot \mathbf{F}(\bar{t}_j) = 0, \quad \mathbf{P}(t) = \mathbf{p} + \mathbf{A}(t), \quad (\text{A1b})$$

where  $\mathbf{p}$  is the final photoelectron momentum,  $\mathbf{A}(t)$  is the laser field vector potential,  $\mathbf{F}(t) = -\partial\mathbf{A}(t)/\partial t$  is the electric field, and

$$S(\mathbf{p}, \bar{t}_j) = \int_{t_0}^{\bar{t}_j} \left\{ \frac{\mathbf{P}(t)^2}{2} + I_p \right\} dt, \quad (\text{A2a})$$

$$\bar{\varkappa}_j = \sqrt{\kappa^2 + \bar{\mathbf{P}}_j^2}, \quad \bar{\mathbf{P}}_j = \mathbf{P}(\bar{t}_j), \quad (\text{A2b})$$

$$\bar{\mathcal{F}}_j = \sqrt{\bar{\mathbf{F}}_j^2 - \bar{\mathbf{P}}_j \cdot \bar{\mathbf{F}}_j}, \quad (\text{A2c})$$

$$\bar{\mathbf{F}}_j = \mathbf{F}(\bar{t}_j), \quad \bar{\dot{\mathbf{F}}}_j = \partial\mathbf{F}(t)/\partial t|_{t=\bar{t}_j}, \quad (\text{A2d})$$

$$f(\mathbf{p}) = \frac{C_\kappa}{2\pi\sqrt{2i\bar{\varkappa}_j\bar{\mathcal{F}}_j}}, \quad \kappa = \sqrt{2I_p}. \quad (\text{A2e})$$

$t_0$  is some constant, whose value does not affect the detachment probability, and  $C_\kappa$  is the asymptotic coefficient for  $s$  initial state  $\psi_0(\mathbf{r})$ :

$$\psi_0(\mathbf{r})|_{\kappa r \gg 1} \simeq \frac{C_\kappa}{\sqrt{4\pi}} \frac{e^{-\kappa r}}{r}.$$

### APPENDIX B: THE “RESCATTERING” AMPLITUDE $\mathcal{A}_j^{(r)}$

The rescattering amplitude  $\mathcal{A}_j^{(r)}(\mathbf{p})$  can be presented as a product of three terms:

$$\mathcal{A}_j^{(r)} = e^{iS(\mathbf{p}, t_j)} a_j^{(\text{tun})} a_j^{(\text{prop})} A(\mathbf{P}_j, \mathbf{K}_j), \quad (\text{B1})$$

where the factor  $a_j^{(\text{tun})}$  describes tunneling step,  $a_j^{(\text{prop})}$  is the propagation factor, describing the semiclassical motion of the liberated electron in the laser-dressed continuum along a closed classical trajectory, and  $A(\mathbf{P}_j, \mathbf{K}_j)$  is the electron-scattering amplitude, describing backscattering on the atomic

residual as the final step in the rescattering mechanism. All these factors depend parametrically on the classical ionization ( $t_j$ ) and recombination ( $t'_j$ ) times, which obey a system of two transcendental equations:

$$\mathbf{K}'_j \cdot \dot{\mathbf{K}}'_j = 0, \quad (\text{B2a})$$

$$\frac{\mathbf{P}^2(t_j)}{2} - \frac{\mathbf{K}_j^2}{2} - \Delta\mathcal{E}_j = 0, \quad (\text{B2b})$$

$$\Delta\mathcal{E}_j = -\frac{\varkappa_j^2}{(t_j - t'_j)\mathcal{F}_j^2} \left[ \frac{\mathbf{K}_j \cdot \mathbf{K}'_j}{t_j - t'_j} - \frac{\mathbf{F}'_j \cdot (\mathbf{K}_j - \mathbf{K}'_j)}{2} \right], \quad (\text{B2c})$$

where  $\kappa = \sqrt{2I_p}$  and

$$\mathbf{K}'_j = \mathbf{A}(t'_j) - \frac{1}{t_j - t'_j} \int_{t'_j}^{t_j} \mathbf{A}(t) dt,$$

$$\mathbf{K}_j = \mathbf{A}(t_j) - \frac{1}{t_j - t'_j} \int_{t'_j}^{t_j} \mathbf{A}(t) dt,$$

$$\dot{\mathbf{K}}'_j = \frac{\partial \mathbf{K}'_j}{\partial t'_j}, \quad \mathcal{F}_j = \sqrt{\mathbf{F}'_j{}^2 - \mathbf{K}'_j \cdot \dot{\mathbf{F}}'_j},$$

$$\varkappa_j = \sqrt{\kappa^2 + \mathbf{K}'_j{}^2}, \quad \mathbf{P}_j = \mathbf{P}(t_j),$$

$$\mathbf{F}'_j = \mathbf{F}(t'_j), \quad \dot{\mathbf{F}}'_j = \frac{\partial \mathbf{F}(t'_j)}{\partial t'_j}.$$

The tunneling and propagation factors can be expressed in the form

$$a_j^{(\text{tun})} = C_\kappa \frac{e^{-\frac{\varkappa_j^3}{3\mathcal{F}_j}}}{\sqrt{4\pi \varkappa_j \mathcal{F}_j}}, \quad (\text{B3})$$

$$a_j^{(\text{prop})} = \sqrt{\frac{2\pi i}{\beta_j}} \frac{e^{iS_j}}{(t_j - t'_j)^{3/2}}, \quad (\text{B4})$$

where

$$S_j = -I_p(t_j - t'_j) - \frac{1}{2} \int_{t'_j}^{t_j} [\mathbf{A}(t) - \mathbf{k}_j]^2 dt,$$

$$\mathbf{k}_j = \frac{1}{t_j - t'_j} \int_{t'_j}^{t_j} \mathbf{A}(t) dt,$$

$$\beta_j = \mathbf{F}_j \cdot (\mathbf{K}_j - \mathbf{P}_j) + \mathbf{K}_j^2/(t_j - t'_j).$$

The scattering amplitude can be presented as an integral involving an exact scattering state,  $\psi_{\mathbf{k}}^{(+)}$  and a plane wave:

$$A(\mathbf{p}, \mathbf{k}) = -\frac{1}{2\pi} \int e^{-i\mathbf{p}\mathbf{r}} U(\mathbf{r}) \psi_{\mathbf{k}}^{(+)}(\mathbf{r}) d\mathbf{r}, \quad (\text{B5})$$

where  $U(\mathbf{r})$  is the atomic potential.

[1] P. Agostini, F. Fabre, G. Mainfray, G. Petite, and N. K. Rahman, Free-Free Transitions Following Six-Photon Ionization of Xenon Atoms, *Phys. Rev. Lett.* **42**, 1127 (1979).

[2] A. T. J. B. Eppink and D. H. Parker, Velocity map imaging of ions and electrons using electrostatic lenses: Application in photoelectron and photofragment ion

- imaging of molecular oxygen, *Rev. Sci. Instrum.* **68**, 3477 (1997).
- [3] J. Ullrich, R. Moshhammer, R. Dörner, O. Jagutzki, V. Mergel, H. Schmidt-Böcking, and L. Spielberger, Recoil-ion momentum spectroscopy, *J. Phys. B: At., Mol. Opt. Phys.* **30**, 2917 (1997).
- [4] D. B. Milošević, G. G. Paulus, D. Bauer, and W. Becker, Above-threshold ionization by few-cycle pulses, *J. Phys. B: At., Mol. Opt. Phys.* **39**, R203 (2006).
- [5] F. Krausz and M. Ivanov, Attosecond physics, *Rev. Mod. Phys.* **81**, 163 (2009).
- [6] W. Becker, S. P. Goreslavski, D. B. Milošević, and G. G. Paulus, The plateau in above-threshold ionization: The keystone of rescattering physics, *J. Phys. B: At., Mol. Opt. Phys.* **51**, 162002 (2018).
- [7] C. Winterfeldt, C. Spielmann, and G. Gerber, Colloquium: Optimal control of high-harmonic generation, *Rev. Mod. Phys.* **80**, 117 (2008).
- [8] E. Hasović, W. Becker, and D. B. Milošević, Electron rescattering in a bicircular laser field, *Opt. Express* **24**, 6413 (2016).
- [9] F. H. M. Faisal, Ionization surprise, *Nat. Phys.* **5**, 319 (2009).
- [10] C. I. Blaga, F. Catoire, P. Colosimo, G. G. Paulus, H. G. Müller, P. Agostini, and L. F. DiMauro, Strong-field photoionization revisited, *Nat. Photonics* **5**, 335 (2009).
- [11] R. A. Ganeev, High-order harmonic generation in a laser plasma: A review of recent achievements, *J. Phys. B: At., Mol. Opt. Phys.* **40**, R213 (2007).
- [12] T. Morishita, A.-T. Le, Z. Chen, and C. D. Lin, Potential for ultrafast dynamic chemical imaging with few-cycle infrared lasers, *New J. Phys.* **10**, 025011 (2008).
- [13] C. D. Lin, A.-T. Le, Z. Chen, T. Morishita, and R. Lucchese, Strong-field rescattering physics – self-imaging of a molecule by its own electrons, *J. Phys. B: At., Mol. Opt. Phys.* **43**, 122001 (2010).
- [14] M.-X. Wang, S.-G. Chen, H. Liang, and L.-Y. Peng, Review on non-dipole effects in ionization and harmonic generation of atoms and molecules, *Chin. Phys. B* **29**, 013302 (2020).
- [15] B. Böning, W. Paufler, and S. Fritzsche, Above-threshold ionization by few-cycle Bessel pulses carrying orbital angular momentum, *Phys. Rev. A* **98**, 023407 (2018).
- [16] W. Paufler, B. Böning, and S. Fritzsche, Strong-field ionization with twisted laser pulses, *Phys. Rev. A* **97**, 043418 (2018).
- [17] P. Ge, Y. Fang, Z. Guo, X. Ma, X. Yu, M. Han, C. Wu, Q. Gong, and Y. Liu, Probing the Spin-Orbit Time Delay of Multiphoton Ionization of Kr by Bicircular Fields, *Phys. Rev. Lett.* **126**, 223001 (2021).
- [18] M. V. Frolov, N. L. Manakov, A. A. Minina, A. A. Silaev, N. V. Vvedenskii, M. Yu. Ivanov, and A. F. Starace, Analytic description of high-order harmonic generation in the adiabatic limit with application to an initial  $s$  state in an intense bicircular laser pulse, *Phys. Rev. A* **99**, 053403 (2019).
- [19] M. V. Frolov, N. L. Manakov, A. A. Minina, N. V. Vvedenskii, A. A. Silaev, M. Yu. Ivanov, and A. F. Starace, Control of Harmonic Generation by the Time Delay Between Two-Color, Bicircular Few-Cycle Mid-IR Laser Pulses, *Phys. Rev. Lett.* **120**, 263203 (2018).
- [20] A. Fleischer, O. Kfir, T. Diskin, P. Sidorenko, and O. Cohen, Spin angular momentum and tunable polarization in high-harmonic generation, *Nat. Photonics* **8**, 543 (2014).
- [21] O. Kfir, P. Grychtol, E. Turgut, R. Knut, D. Zusin, D. Popmintchev, T. Popmintchev, H. Nembach, J. M. Shaw, A. Fleischer, H. Kapteyn, M. Murnane, and O. Cohen, Generation of bright phase-matched circularly-polarized extreme ultraviolet high harmonics, *Nat. Photonics* **9**, 99 (2015).
- [22] C. A. Mancuso, D. D. Hickstein, P. Grychtol, R. Knut, O. Kfir, X.-M. Tong, F. Dollar, D. Zusin, M. Gopalakrishnan, C. Gentry, E. Turgut, J. L. Ellis, M.-C. Chen, A. Fleischer, O. Cohen, H. C. Kapteyn, and M. M. Murnane, Strong-field ionization with two-color circularly polarized laser fields, *Phys. Rev. A* **91**, 031402 (2015).
- [23] C. A. Mancuso, K. M. Dorney, D. D. Hickstein, J. L. Chaloupka, X.-M. Tong, J. L. Ellis, H. C. Kapteyn, and M. M. Murnane, Observation of ionization enhancement in two-color circularly polarized laser fields, *Phys. Rev. A* **96**, 023402 (2017).
- [24] D. Milošević, Atomic and molecular processes in a strong bicircular laser field, *Atoms* **6**, 61 (2018).
- [25] P.-C. Huang, C. Hernández-García, J.-T. Huang, P.-Y. Huang, C.-H. Lu, L. Rego, D. D. Hickstein, J. L. Ellis, A. Jaron-Becker, A. Becker, S.-D. Yang, C. G. Durfee, L. Plaja, H. C. Kapteyn, M. M. Murnane, A. H. Kung, and M.-C. Chen, Polarization control of isolated high-harmonic pulses, *Nat. Photonics* **12**, 349 (2018).
- [26] K. M. Dorney, T. Fan, Q. L. D. Nguyen, J. L. Ellis, D. D. Hickstein, N. Brooks, D. Zusin, C. Gentry, C. Hernández-García, H. C. Kapteyn, and M. M. Murnane, Bright, single helicity, high harmonics driven by mid-infrared bicircular laser fields, *Opt. Express* **29**, 38119 (2021).
- [27] L. V. Keldysh, Ionization in the field of a strong electromagnetic wave, *Zh. Eksp. Teor. Fiz.* **47**, 1945 (1964) [*J. Exp. Theor. Phys.* **20**, 1307 (1965)].
- [28] F. H. M. Faisal, Multiple absorption of laser photons by atoms, *J. Phys. B: At. Mol. Phys.* **6**, L89 (1973).
- [29] H. R. Reiss, Effect of an intense electromagnetic field on a weakly bound system, *Phys. Rev. A* **22**, 1786 (1980).
- [30] V. S. Popov, Tunnel and multiphoton ionization of atoms and ions in a strong laser field (Keldysh theory), *Usp. Fiz. Nauk* **174**, 921 (2004) [*Phys.-Usp.* **47**, 855 (2004)].
- [31] S. V. Popruzhenko, Keldysh theory of strong field ionization: History, applications, difficulties and perspectives, *J. Phys. B: At., Mol. Opt. Phys.* **47**, 204001 (2014).
- [32] O. I. Tolstikhin and T. Morishita, Adiabatic theory of ionization by intense laser pulses: Finite-range potentials, *Phys. Rev. A* **86**, 043417 (2012).
- [33] Y. Okajima, O. I. Tolstikhin, and T. Morishita, Adiabatic theory of high-order harmonic generation: One-dimensional zero-range-potential model, *Phys. Rev. A* **85**, 063406 (2012).
- [34] A. V. Flegel, N. L. Manakov, A. V. Sviridov, M. V. Frolov, L. Geng, and L.-Y. Peng, Analytic description of the above-threshold detachment in the adiabatic limit, *Phys. Rev. A* **102**, 063119 (2020).
- [35] A. V. Flegel, N. L. Manakov, I. V. Breev, and M. V. Frolov, Adiabatic expressions for the wave function of an electron in a finite-range potential and an intense low-frequency laser pulse, *Phys. Rev. A* **104**, 033109 (2021).
- [36] M. V. Frolov, N. L. Manakov, E. A. Pronin, and A. F. Starace, Model-Independent Quantum Approach for Intense Laser Detachment of a Weakly Bound Electron, *Phys. Rev. Lett.* **91**, 053003 (2003).

- [37] B. M. Karnakov, V. D. Mur, S. V. Popruzhenko, and V. S. Popov, Current progress in developing the nonlinear ionization theory of atoms and ions, *Usp. Fiz. Nauk* **185**, 3 (2015) [*Phys.-Usp.* **58**, 3 (2015)].
- [38] S. V. Popruzhenko and D. Bauer, Strong field approximation for systems with Coulomb interaction, *J. Mod. Opt.* **55**, 2573 (2008).
- [39] C. Figueira de Morisson Faria and A. S. Maxwell, It is all about phases: Ultrafast holographic photoelectron imaging, *Rep. Prog. Phys.* **83**, 034401 (2020).
- [40] T.-M. Yan, S. V. Popruzhenko, M. J. J. Vrakking, and D. Bauer, Low-Energy Structures in Strong Field Ionization Revealed by Quantum Orbits, *Phys. Rev. Lett.* **105**, 253002 (2010).
- [41] C. Liu and K. Z. Hatsagortsyan, Origin of Unexpected Low Energy Structure in Photoelectron Spectra Induced by Midinfrared Strong Laser Fields, *Phys. Rev. Lett.* **105**, 113003 (2010).
- [42] A. Kästner, U. Saalmann, and J. M. Rost, Electron-Energy Bunching in Laser-Driven Soft Recollisions, *Phys. Rev. Lett.* **108**, 033201 (2012).
- [43] S. V. Popruzhenko, Coulomb phase in high harmonic generation, *J. Phys. B: At., Mol. Opt. Phys.* **51**, 144006 (2018).
- [44] M. V. Frolov, N. L. Manakov, A. A. Minina, S. V. Popruzhenko, and A. F. Starace, Adiabatic-limit Coulomb factors for photoelectron and high-order-harmonic spectra, *Phys. Rev. A* **96**, 023406 (2017).
- [45] J. Dubois, S. A. Berman, C. Chandre, and T. Uzer, Capturing Photoelectron Motion with Guiding Centers, *Phys. Rev. Lett.* **121**, 113202 (2018).
- [46] U. S. Sainadh, H. Xu, X. Wang, A. Atia-Tul-Noor, W. C. Wallace, N. Douguet, A. Bray, I. Ivanov, K. Bartschat, A. Kheifets, R. T. Sang, and I. V. Litvinyuk, Attosecond angular streaking and tunnelling time in atomic hydrogen, *Nature (London)* **568**, 75 (2019).
- [47] S. V. Popruzhenko, Invariant form of Coulomb corrections in the theory of nonlinear ionization of atoms by intense laser radiation, *Zh. Eksp. Teor. Fiz.* **145**, 664 (2014) [*J. Exp. Theor. Phys.* **118**, 580 (2014)].
- [48] L.-Y. Peng, W.-C. Jiang, J.-W. Geng, W.-H. Xiong, and Q. Gong, Tracing and controlling electronic dynamics in atoms and molecules by attosecond pulses, *Phys. Rep.* **575**, 1 (2015).
- [49] G. G. Paulus, W. Becker, W. Nicklich, and H. Walther, Rescattering effects in above-threshold ionization: A classical model, *J. Phys. B: At., Mol. Opt. Phys.* **27**, L703 (1994).
- [50] R. G. Newton, *Scattering Theory of Waves and Particles*, 2nd ed. (Springer Science & Business Media, 2013), p. 745.
- [51] B. M. Smirnov and M. I. Chibisov, The breaking up of atomic particles by an electric field and by electron collisions, *Zh. Eksp. Teor. Fiz.* **49**, 841 (1965) [*Sov. Phys. JETP* **22**, 585 (1966)].
- [52] A. M. Perelomov and V. S. Popov, Ionization of atoms in an alternating electrical field. III, *Zh. Eksp. Teor. Fiz.* **52**, 514 (1967) [*J. Exp. Theor. Phys.* **25**, 336 (1967)].
- [53] Ph. A. Korneev, S. V. Popruzhenko, S. P. Goreslavski, W. Becker, G. G. Paulus, B. Fetić, and D. B. Milošević, Interference structure of above-threshold ionization versus above-threshold detachment, *New J. Phys.* **14**, 055019 (2012).
- [54] Th. Keil, S. V. Popruzhenko, and D. Bauer, Laser-Driven Recollisions under the Coulomb Barrier, *Phys. Rev. Lett.* **117**, 243003 (2016).
- [55] L. Torlina and O. Smirnova, Coulomb time delays in high harmonic generation, *New J. Phys.* **19**, 023012 (2017).
- [56] T. N. Rescigno and C. W. McCurdy, Numerical grid methods for quantum-mechanical scattering problems, *Phys. Rev. A* **62**, 032706 (2000).
- [57] Tae Jun Park and J. C. Light, Unitary quantum time evolution by iterative Lanczos reduction, *J. Chem. Phys.* **85**, 5870 (1986).
- [58] X. M. Tong, K. Hino, and N. Toshima, Phase-dependent atomic ionization in few-cycle intense laser fields, *Phys. Rev. A* **74**, 031405(R) (2006).
- [59] X.-Y. Lai, C. Poli, H. Schomerus, and C. Figueira de Morisson Faria, Influence of the Coulomb potential on above-threshold ionization: A quantum-orbit analysis beyond the strong-field approximation, *Phys. Rev. A* **92**, 043407 (2015).
- [60] X.-Y. Lai, S.-G. Yu, Y.-Y. Huang, L.-Q. Hua, C. Gong, W. Quan, C. Figueira de Morisson Faria, and X.-J. Liu, Near-threshold photoelectron holography beyond the strong-field approximation, *Phys. Rev. A* **96**, 013414 (2017).
- [61] A. S. Maxwell, S. V. Popruzhenko, and C. Figueira de Morisson Faria, Treating branch cuts in quantum trajectory models for photoelectron holography, *Phys. Rev. A* **98**, 063423 (2018).
- [62] L. D. Landau and E. M. Lifshitz, *Quantum Mechanics (Non-Relativistic Theory)* (Pergamon Press, Oxford, 1977).
- [63] M. V. Frolov, D. V. Knyazeva, N. L. Manakov, J.-W. Geng, L.-Y. Peng, and A. F. Starace, Analytic model for the description of above-threshold ionization by an intense short laser pulse, *Phys. Rev. A* **89**, 063419 (2014).